Original articles

# Dynamic finite element analysis and moving particle simulation of human enamel on a micro scale

Satoshi Yamaguchi[a*], Paulo G Coelho[b], Van P Thompson[c], Nick Tovar[b], Junpei Yamauchi[a], Satoshi Imazato[a]

[a] Department of Biomaterials Science, Osaka University Graduate School of Dentistry, 1-8 Yamadaoka, Suita, Osaka 565-0871, Japan

[b] Department of Biomaterials and Biomimetics, New York University College of Dentistry, 345 E 24th Street, New York, NY, 10010, USA

[c] Department of Biomaterials, Biomimetics and Biophotonics, King's College London, Dental Institute, Guy's Hospital, London, SE1 9RT, UK

*Correspondence should be addressed to Satoshi Yamaguchi

Department of Biomaterials Science, Osaka University

1-8 Yamadaoka, Suita, Osaka 565-0871, Japan

1 Tel/Fax: +81-6-6879-2919

2 Email: yamagu@dent.osaka-u.ac.jp

3

4 Number of reprints: 5

5

## ABSTRACT

**Background:** The study of biomechanics of deformation and fracture of hard biological tissues involving organic matrix remains a challenge as variations in mechanical properties and fracture mode may have time-dependency. Finite element analysis (FEA) has been widely used but the shortcomings of FEA such as the long computation time owing to re-meshing in simulating fracture mechanics have warranted the development of alternative computational methods with higher throughput. The aim of this study was to compare dynamic two-dimensional FEA and moving particle simulation (MPS) when assuming a plane strain condition in the modeling of human enamel on a reduced scale.

**Methods:** Two-dimensional models with the same geometry were developed for MPS and FEA and tested in tension generated with a single step of displacement. The displacement, velocity, pressure, and stress levels were compared and Spearman's rank-correlation coefficients R were calculated ($p$<0.001).

**Results:** The MPS and FEA were significantly correlated for displacement, velocity, pressure, and Y-stress.

**Conclusions:** The MPS may be further developed as an alternative approach without mesh generation to simulate deformation and fracture phenomena of dental and potentially other

1 hard tissues with complex microstructure.

2

3 **Keywords:** dental enamel, finite element analysis, computer simulation

4

5

## INTRODUCTION

Understanding the biomechanics of deformation and fracture of biological tissues is crucial in not only elucidating tissue damage caused by external forces but also in developing novel biomaterials for tissue substitution. Native biological tissues have a variety of mechanical properties even within a single tissue [1], because the cell and matrix distributions are different within the tissue and each has time-dependent property variation. Therefore, the precise measurement of the deformation and complex fracture patterns of biological tissues remains a major challenge [2]. Finite element analysis (FEA) [3, 4] is considered an important tool with which to elucidate the biomechanics of such deformation [5] and fracture [6].

While FEA has been widely used in dentistry to simulate different treatment modalities that are dental or implant supported, the mechanical simulation of dental tissue deformation and fracture has received notably less attention. One of the reasons for such a lack of data in the literature is the challenge of properly modeling the complex structure of enamel and dentin micro structures [7, 8], the dentin-enamel-junction [9], and the hybrid layer [10]. Among them, enamel is an especially-important target for the elucidation of the biomechanics of fracture because of its complex deformation patterns and principal modes of tooth failures, which include radial/median cracking and channel-like margin cracking [11].

Enamel has a complex microstructure involving organic matter surrounded by a tufts-like structure and both viscoelastic and viscoplastic behavior to make wear resistance, anti-fatigue, and crack resistant abilities [12].

The usual assumption of small deformation commonly made for FEA software meshes results in a geometric limitation when attempting to evaluate large deformation and fracture. Especially in the simulation of crack propagation, mesh elimination techniques of Lagrangian based FEA, which generate complex boundary conditions, are used. Thus, to predict fracture phenomena precisely, a finite element model must be presented on a number of meshes throughout time, further increasing the time required for simulation. In general, when modeling intricate functionally graded complex geometries such as those of enamel and dentin, the approximation error is reduced by refining the mesh. Computations thus need to be made for multiple mesh iteration in systems undergoing deformations. The development of new approaches of simulating dental tissues would be beneficial to researchers and ultimately clinicians and patients as an improvement in the mechanical simulation of such tissues would allow a more robust informed design platform for the development of novel biomaterials and treatment modalities.

Moving particle simulation (MPS) is a computational method of simulating the

fragmentation of incompressible free surface flows originally used in nuclear engineering [13]. Recently, the MPS has been extended to the non-linear elastodynamics of compressible and incompressible materials such as viscosity in enamel [14]. When compared with FEA, MPS has the distinct advantage of being a mesh free model, which is more suited to deformation analysis and to simulation of complex material properties such as interprismatic organic matrix of enamel [15]. A current limitations of the MPS method is that to date there have been no systematic comparative studies with FEA.

The aim of this study was to perform dynamic two-dimensional FEA and MPS micro scale modeling of human enamel in a single layer assuming a plane strain condition as a basic evaluation. Two-dimensional models with the same geometry were developed for both MPS and FEA and the models were tested in tension. The displacement, velocity, pressure, and stress levels were compared between the two simulation methods.

## MATERIALS AND METHODS

*Elastic foundation of moving particle simulation*

In MPS [13], the constitutive equation in terms of velocity for an elastic body $v^{\alpha}$ is follows:

$$\rho \frac{\partial v^{\alpha}}{\partial t} = \frac{\partial}{\partial x^{\beta}} \left[ \lambda \varepsilon^{\gamma\gamma} \delta^{\alpha\beta} + 2\mu \varepsilon^{\alpha\beta} \right] \quad (1)$$

where $\rho$, $\varepsilon^{\gamma\gamma}$, and $\delta^{\alpha\beta}$ are the density, volumetric strain, and Kronecker delta, respectively. $\alpha$, $\beta$, and $\gamma$ are the axis directions. $\boldsymbol{x}$ is the position of a particle. $\lambda$ and $\mu$ are Lame constants and relate to Young's modulus $E$ and Poisson's ratio $\upsilon$, which are defined by the following equations.

$$\lambda = \frac{E\upsilon}{(1+\upsilon)(1-2\upsilon)} \quad (2)$$

$$\mu = \frac{E}{2(1+\upsilon)} \quad (3)$$

In MPS, the partial differential equation is discretized using a model of interaction between particles. The interaction model takes the form of a weight function $W$:

$$W(r_{ij}) = \begin{cases} \frac{r_e}{r_{ij}} - 1 & (r_{ij} \le r_e) \\ 0 & (r_{ij} > r_e) \end{cases}, \quad (4)$$

where $r_{ij}$ is the distance between particles $i$ and $j$ and $r_e$ is the affected radius of particle $i$. The initial relative position $\boldsymbol{r}_{ij0}$ and relative position during calculation $\boldsymbol{r}_{ij}$ between particle $i$ and $j$ are defined as

$$\boldsymbol{r}_{ij0} = \boldsymbol{x}_{j0} - \boldsymbol{x}_{i0} \tag{5}$$

$$\boldsymbol{r}_{ij} = \boldsymbol{x}_{j} - \boldsymbol{x}_{i} \tag{6}$$

where $\boldsymbol{x}_{j0}$ and $\boldsymbol{x}_{i0}$ and $\boldsymbol{x}_{j}$ and $\boldsymbol{x}_{i}$ are an initial and current position vectors for particles $j$ and $i$, respectively. Let $\boldsymbol{r}_{\theta}$ be a rotated vector such that $\boldsymbol{r}_{ij0}$ was rotated through an angle $\theta_{ij}$:

$$\boldsymbol{r}_{\theta} = T_{ij} \cdot \boldsymbol{r}_{ij0}. \tag{7}$$

Here, $\boldsymbol{T}_{ij}$ and $\theta_{ij}$ are defined by

$$T_{ij} = \begin{bmatrix} \cos\theta_{ij} & -\sin\theta_{ij} \\ \sin\theta_{ij} & \cos\theta_{ij} \end{bmatrix}, \tag{8}$$

$$\theta_{ij} = \frac{\theta_i - \theta_j}{2}. \tag{9}$$

By subtracting $\boldsymbol{r}_{\theta}$ from $\boldsymbol{r}_{ij}$, the relative displacement vector due to strain $\boldsymbol{u}_{ij}^{\varepsilon}$ is obtained as

$$\boldsymbol{u}_{ij}^{\varepsilon} = \boldsymbol{r}_{ij} - \boldsymbol{r}_{\theta}. \tag{10}$$

This relative displacement vector is divided into normal and tangential directions:

$$\left(\boldsymbol{u}_{ij}^{\varepsilon}\right)^{n} = \frac{\left(\boldsymbol{u}_{ij}^{\varepsilon} \cdot \boldsymbol{r}_{ij}\right)\boldsymbol{r}_{ij}}{\left|\boldsymbol{r}_{ij}^{2}\right|}, \tag{11}$$

$$\left(\boldsymbol{u}_{ij}^{\varepsilon}\right)^{s} = \boldsymbol{u}_{ij}^{\varepsilon} - \left(\boldsymbol{u}_{ij}^{\varepsilon}\right)^{n}. \tag{12}$$

Normal and tangential components of the tensor of strain between particles $i$ and $j$ are

$$\left(\varepsilon^{n}\right)_{ij} = \frac{\left(\boldsymbol{u}_{ij}^{\varepsilon}\right)^{n}}{\left|\boldsymbol{r}_{ij0}\right|}, \tag{13}$$

$$\left(\varepsilon^{s}\right)_{ij} = \frac{\left(\boldsymbol{u}_{ij}^{\varepsilon}\right)^{s}}{\left|\boldsymbol{r}_{ij0}\right|}. \qquad (14)$$

Finally, normal and shear stress $\sigma_{ij}$ and $\tau_{ij}$ are calculated as.

$$\sigma_{ij} = 2\mu\left(\varepsilon^{n}\right)_{ij} = 2\mu\frac{\left(\boldsymbol{u}_{ij}^{\varepsilon}\right)^{n}}{\left|\boldsymbol{r}_{ij0}\right|}, \qquad (15)$$

$$\tau_{ij} = 2\mu\left(\varepsilon^{s}\right)_{ij} = 2\mu\frac{\left(\boldsymbol{u}_{ij}^{\varepsilon}\right)^{s}}{\left|\boldsymbol{r}_{ij0}\right|}. \qquad (16)$$

*Development of finite element and moving particle model*

A two-dimensional finite element model were constructed for human enamel by assuming plane strain conditions as shown in **Fig. 1**. The two models had identical model geometry, boundary conditions, material properties. The time scale was also identical between models. The numbers of nodes (FEA) and particles (MPS) were 462 (11 × 42). The nodes and particles were regularly spaced at intervals of 3μm. The nodes and particles in a 11 × 3 configuration in the upper and lower aspects of the model were set as rigid bodies while the middle part was set as a linear elastic body with the mechanical properties of enamel (Young's modulus: 84.1 GPa, Poisson's ratio of 0.3 [16], and density of 3000 kg/m$^3$ [17]). By following the compression loading on the macro scale, the lower rigid body was completely fixed and the upper rigid body was tensioned in the y-direction by applying a displacement of 0.76 μm

in one step. Rigid bodies of upper and lower part was adopted to maintain a numerical stability. The total simulation time was adjusted to 3.0e–6 s, which was sufficient time to observe single stress propagation from the top to the bottom of the model. Both FEA and MPS were performed as dynamic analysis with time dependency.

*FEA and MPS*

To evaluate the difference between FEA and MPS, the displacement, velocity, pressure, and Y-stress (stress along the Y axis, **Fig. 2**) output were observed from step 0 to 3000 in intervals of 600 steps. For the displacement and velocity, nodes 35 and 238; and particles 407 and 214 were selected as observation points (**Fig. 2A**), respectively. For the pressure and Y-stress, elements 21 and 184; and particle 407 and the average of particle 202, 203, 213, and 214 were selected as observation areas (**Fig. 2B**). Then, maximum differences for each parameter along the entire simulation time frame were then determined and Spearman's coefficient R for rank correlation between MPS and FEA was calculated ($p$<0.001) using SPSS Statistics 18 (IBM-SPSS, Chicago, IL, USA). For each parameter evaluated at different regions of the specimen. FEA was performed by LS-DYNA (LSTC, Livermore, CA, USA) and MPS was originally implemented using C++ language in Visual Studio 2010 Express

1 Edition (Microsoft, Minato-ku, Japan). FEA and MPS software ran on a single custom-made
2 workstation (Windows 7 Professional Service Pack 1 64bit OS, 24GB RAM, Intel(R)
3 Xeon(R) W5590 3.33GHz CPU) to avoid workstation variability and the calculation cost (run
4 time, CPU usage, and working memory usage) was recorded. Finally, the Y-stress distribution
5 plots and measured velocities of stress propagation from displacement of 0.099 mm between
6 elements 22 and 55; and particles 407 and 33 were obtained.
7

## RESULTS

*Displacement*

**Figure 3A** and **3B** shows the results for displacement at node 35 (N35) and particle 407 (P407) in x and y direction, respectively. **Figure 3C** shows the result of displacement at node 238 (N238) and particle 214 (P214) in the y direction. No displacement was observed in the x direction.

*Velocity*

**Figure 3D** and **3E** shows the results for velocity at N35 and P407 in the x and y directions, respectively. **Figure 3F** and **3G** shows the results for velocity at N238 and P214 in x and y directions, respectively.

*Pressure*

**Figure 4A** shows the result for pressure at element 22 (E22) and the average for particles 396, 397, 407, and 408 (P396-397-407-408). **Figure 4B** shows the result for pressure at element 220 (E220) and the average for particles 203, 204, 214, and 215 (P203-204-214-215).

*Y-stress and Y-stress distribution and propagation*

**Figure 4C** shows the result for Y-stress at E22 and the average of normal stress at

P396-397-407-408. **Figure 4D** shows the result for Y-stress at E220 and the average of normal stress at P203-204-214-215. **Figure 5** shows the results for the Y-stress distribution in FEA and MPS. The color bars for FEA and MPS have a range of 0.0–0.6 MPa (**Fig. 5A**) and 0.0–0.9 MPa (**Fig. 5B**), respectively. The maximum Y-stresses of FEA and MPS were 1.353 MPa at element 380 (time = 2.7540e–5 s, x = 0.0285 mm, y = 0.00750 mm) and 1.643 MPa at particle 115 (time = 2.6619e–5 s, x = 0.0150 mm, y = 0.0300 mm). The velocities of Y-stress propagation in FEA and MPS were 3831 and 4716 m/s, respectively.

*Maximum differences and Spearman's rank-correlation coefficients R*

**Table 1** shows the maximum differences between MPS and FEA for displacement, velocity, pressure, and Y-stress. **Table 2** shows the Spearman's rank-correlation coefficients R between MPS and FEA for displacement, velocity, pressure, and Y-stress.

*Calculation cost*

Run times of FEA and MPS were 4 s and 4 min 17 s, respectively. CPU use in FEA and MPS was 7.05 % for eight threads (0.881 % for one thread) and 12.5 % for one thread, respectively. Working memory usage in FEA and MPS was 230,458 KB and 7960 KB, respectively.

## DISCUSSION

Simulations were performed under the assumption of dental enamel being a linear elastic isotropic material and that there is no attenuation of the elastic wave. The results obtained from FEA and MPS had overall agreement, indicating that MPS is a suitable tool for dynamic structural and mechanical simulation. The assumption of plane strain in two dimensions was made because dental enamel has longitudinal structures (the enamel rods) throughout its thickness. Given that current imaging techniques allow high-resolution three-dimensional reconstruction of mineralized tissue structures, MPS may be used for mechanical simulation because each particle may be made to correspond to each imaging pixel [18]. Because three-dimensional reconstruction has become more readily available, voxel-based FEA [19-21] has been carried out to analyze complex microstructure such as human trabecular bone. However, reconstructing models through meshing imaging is a challenge as high degrees of refinement are required prior to final computation. In recent years, the mesh free method [22] has provided promising results for deformation as seen in neurosurgical simulation [23]. However, dynamic and fracture analysis still remains a major challenge because this approach involves time-consuming tasks including a huge matrix calculation that is comparable to calculations in FEA. In contrast, MPS is attractive because

of its easy implementation for the mechanical simulation of deformation and potentially the analysis of fracture mechanics of complex structures.

MPS allows for the use of self-implemented programming without the need for cost-prohibitive optimization. The algorithm within MPS can be expanded and use GPGPU technology can be used [24]. The results of the present study show that the working memory usage of MPS was dramatically low (3.454 %) in comparison with that of FEA; therefore, MPS was far more efficient than FEA in terms of using computer resources. MPS had longer run time and CPU time, which can be effectively decreased if working memory is added at the same level as in FEA.

Simulations were successfully carried out using the two constructed models and compared in terms of displacement, velocity, pressure, and Y-stress propagation. While there were differences between FEA and MPS results in terms of oscillations resulting from the two different approaches as described by equations 15 and 16 for discretization of the continuum model in equation 1, the trends observed were remarkably similar for most of the parameters evaluated. The displacement results observed were statistically (high R values) similar excluding the x-displacement. In the case of P407, we speculate that the upper particles of the rigid body were excluded in the calculation of x-displacement while N35 was considered as a

Gauss integral point. The same could be said for y-displacement. However, the scale of y-displacement was approximately 40 times that of x-displacement. Additionally, the maximum difference in x-displacement of 4.513e–9 mm was considerably less than the width of the model of 0.03 mm and thereby potentially acceptable. These results suggest that a strain threshold derived using equation 13 and 14 should be adopted in future simulations of fracture or failure. For this purpose, the maximum principal strain may be a useful as fracture criterion as it is known to be an effective criterion for brittle materials such as the human femur [25] and enamel [26].

There was no displacement at node 238 and particle 214 in the x direction because the node and particle were located at the centroids of the two models. The oscillation in the Y-velocity output of the MPS was possibly affected by the equations used, which described mechanical springs acting between particles despite MPS was not being implemented as a mass–spring model. The oscillation cycle is commonly related with a spring coefficient and a mass point (mass of a particle in the case of MPS). The Spearman's rank-correlation coefficients for x-velocity were lower than those for y-velocity. In the case of P407, the low Spearman's rank-correlation coefficient is possibly related to the above-mentioned differences in the x-displacement results. In the other case, the erratic X-velocity output of the FEA

would also be zero once an integral of the curve is taken. One reason for such oscillation may be truncation error related to the quite small values obtained. Pressure obtained for both models had negative values typically observed in tension tests. The Y-stress results had a sharp peak and three peaks of lower magnitude in both FEA and MPS. The difference in the peaks likely arose from the difference in the calculation methods for Y-stress between the methods. In the case of FEA, the average of Y-stress for four Gauss integral points in one element that consist of four nodes is calculated. Meanwhile, MPS uses 12 particles within an influence radius (equation 4) to calculate Y-stress at one particle and the average for four particles is then calculated. Spearman's coefficients for rank correlation between pressure and Y-stress were lower for P396-397-407-408 than for P203-204-214-215. These results are the result of the averaging effect and the above-mentioned difference in the x-displacement results. To reduce such differences, the reconstruction of models with higher resolution may be effective.

The velocity of stress propagation in the MPS was higher than in FEA and a theoretical velocity of 5192 m/s. In obtaining the theoretical velocity of stress propagation, we used a P wave, which has higher velocity in the direction of forward movement than P, S, head, and Rayleigh waves. This result suggests that the trajectories of stress propagation

could possibly be simulated even during fracture in MPS.

For more realistic and complex situations that could better simulated by MPS, we are ongoing to develop three-dimensional enamel micro structure with anisotropic enamel sheath and interprismatic organic matrix as the next stage.

## CONCLUSION

Within the limitation of two-dimensional analysis, we successfully applied MPS to human enamel tissue at a micro scale and compared displacement, velocity, pressure, and Y-stress results with the results of FEA. The implemented MPS provided results highly correlated to FEA and it may be extended to other hard biological tissues involving soft organic matrix.

## ACKNOWLEDGEMENTS

This study was supported by a Grant-in-Aid for Scientific Research (No. 24592955) from the Japan Society for the Promotion of Science. The authors thank Prof. Seiichi Koshizuka and Prof. Kazuya Shibata at Tokyo University for advice of the implementation of MPS. The authors declare no potential conflicts of interest with respect to the authorship and/or publication of this article.

## AUTHOR CONTRIBUTIONS

SY conceived and designed the experiments. SY performed the simulations. SY analyzed the data. SY and JY contributed materials/analysis tools. SY, PC, VP, and NT wrote the paper. VT and SI provided administrative support.

## REFERENCES


1. Lam RH, Weng S, Lu W. Fu J, Live-cell subcellular measurement of cell stiffness using a microengineered stretchable micropost array membrane. *Integr Biol* 4 (2012) 1289-1298.

2. Keller PJ, Schmidt AD, Wittbrodt J. Stelzer EH, Reconstruction of zebrafish early embryonic development by scanned light sheet microscopy. *Science* 322 (2008) 1065-1069.

3. Turner MJ, Clough RW, Martin HC. Topp LJ, Stiffness and Deflection Analysis of Complex Structures. *J Aeronaut Sci* 23 (1956) 805-823.

4. Zienkiewicz C, The birth of the finite element method and of computational mechanics. *Int J Numer Meth Eng* 60 (2004) 3-10.

5. Slomka N, Gefen A, Confocal microscopy-based three-dimensional cell-specific modeling for large deformation analyses in cellular mechanics. *J Biomech* 43 (2010) 1806-1816.

6. Stolk J, Verdonschot N, Mann KA, Huiskes R, Prevention of mesh-dependent damage growth in finite element simulations of crack formation in acrylic bone cement. *J Biomech* 36 (2003) 861-871.

7. Kinnery JH, Marshall SJ, Marshall GW, The mechanical properties of human dentin: a critical review and re-evaluation of the dental literature. *Crit Rev Oral Biol Med* 14 (2003) 13-29.

8. He LH, Swain MV, Understanding the mechanical behaviour of human enamel from its structural and compositional characteristics. *J Mech Behav Biomed Mater* 1 (2008) 18-29.

9. White SN, Paine ML, Luo W, Sarikaya M, Fong H, Yu ZK, et al., The dentino-enamel junction is a broad transitional zone uniting dissimilar bioceramic composites. *J Am Ceram Soc* 83 (2000) 238-240.

10. Nakabayashi N, The hybrid layer: a resin-dentin composite. *Proc Finn Dent Soc* 88 (Suppl

1) (1992) 321-329.

11. Myoung S, Lee J, Constantino P, Lucas P, Chai H, Lawn B, Morphology and fracture of enamel. *J Biomech* 42 (2009) 1947-1951.

12. He LH, Swain MV, Nanoindentation creep behavior of human enamel. *J Biomed Mater Res A* 91 (2009) 352-359.

13. Koshizuka S, Oka Y, Moving-particle semi-implicit method for fragmentation of incompressible fluid. *Nucl Sci Eng* 123 (1996) 421-434.

14. Suzuki Y, Koshizuka S, A Hamiltonian particle method for non-linear elastodynamics. *Int J Numer Meth Eng* 74 (2008) 1344-1373.

15. Zheng Q, Xu H, Song F, Zhang L, Zhou X, Shao Y, Huang, Spatial distribution of the human enamel fracture toughness with aging. *J Mech Behav Biomed Mater* (doi: 10. 1016/j.jmbbm.2013.04.025) (2013) 148-154.

16. Magne P, Virtual prototyping of adhesively restored, endodontically treated molars. *J Prosthet Dent* 103 (2010) 343-351.

17. Ghorayeb SR, Xue T, Lord W, A finite element study of ultrasonic wave propagation in a tooth phantom. *J Dent Res* 77 (1998) 39-49.

18. Ryou H, Niu LN, Dai L, Pucci CR, Arola DD, Pashley DH, et al., Effect of biomimetic remineralization on the dynamic nanomechanical properties of dentin hybrid layers. *J Dent Res* 90 (2011) 1122-1128.

19. Adachi T, Tsubota K, Tomita Y, Hollister SJ, Trabecular surface remodeling simulation for cancellous bone using microstructural voxel finite element models. *J Biomech Eng-T Asme* 123 (2001) 403-409.

20. Mishnaevsky LL, Automatic voxel-based generation of 3D microstructural FE models and its application to the damage analysis of composites. *Mat Sci Eng a-Struct* 407 (2005)

11-23.

21. Fagan MJ, Curtis N, Dobson CA, Karunanayake JH, Kitpczik K, Moazen M, et al., Voxel-based finite element analysis - Working directly with microCT scan data. *J Morphol* 268 (2007) 1071-1071.

22. Horton A, Wittek A, Jolders GR, Miller K, A meshless Total Lagrangian explicit dynamics algorithm for surgical simulation. *Int J Numer Meth Bio* 26 (2010) 977-998.

23. Miller K, Horton A, Jolders GR, Wittek A, Beyond finite elements: a comprehensive, patient-specific neurosurgical simulation utilizing a meshless method. *J Biomech* 45 (2012) 2698-2701.

24. Hori C, Gotoh H, Ikari H, Khayyer A, GPU-acceleration for Moving Particle Semi-Implicit method. *Comput Fluids* 51 (2011) 174-183.

25. Schileo E, Taddei F, Cristofolini L, Viceconti M, Subject-specific finite element models

implementing a maximum principal strain criterion are able to estimate failure risk and fracture location on human femurs tested in vitro. *J Biomech* 41 (2008) 356-367.

26. Anderson PS, Gill PG, Rayfield EJ, Modeling the effects of cingula structure on strain patterns and potential fracture in tooth enamel. *J Morphol* 272 (2011) 50-65.

**Figure**

Figure 1

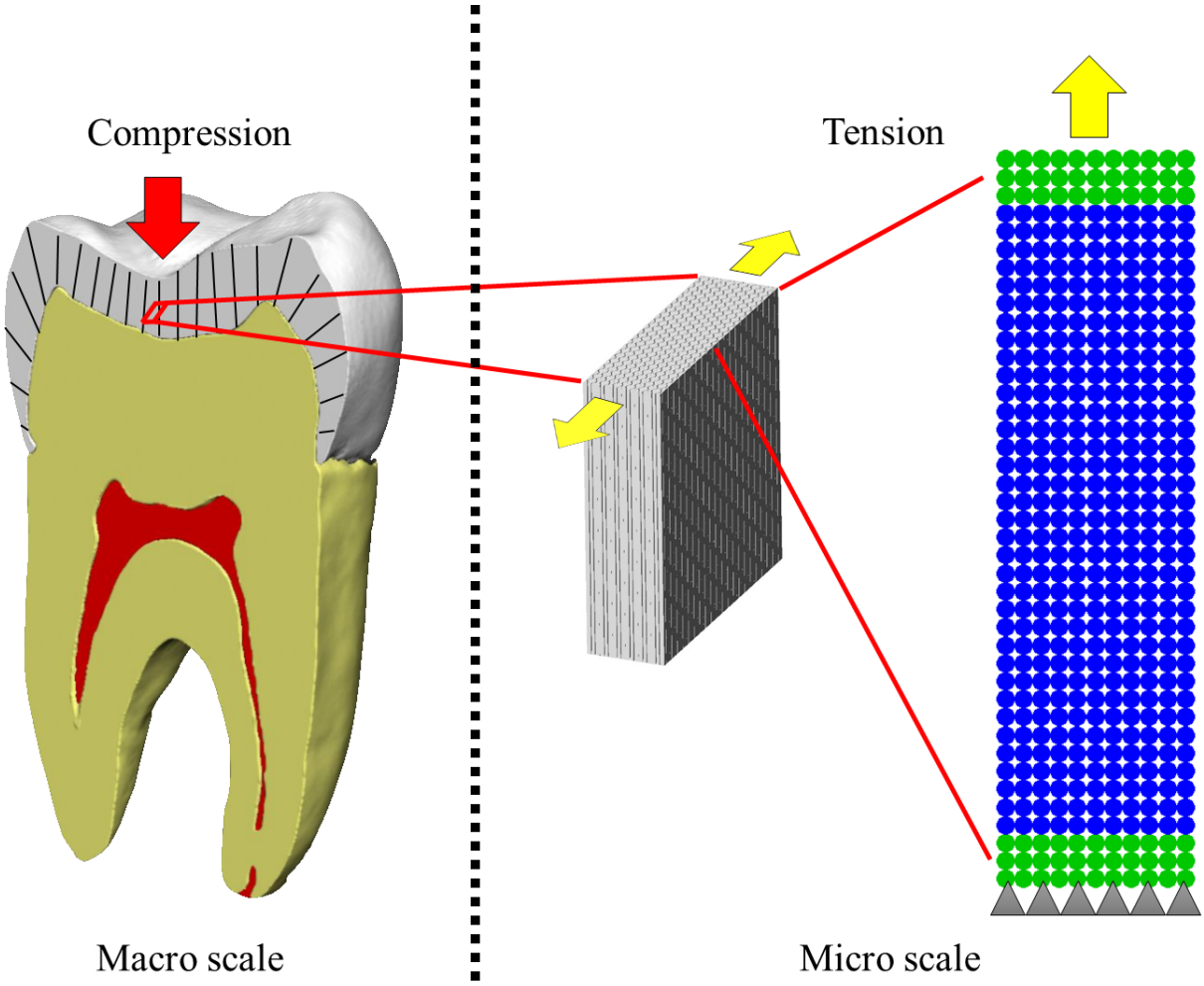

Figure 2(A)

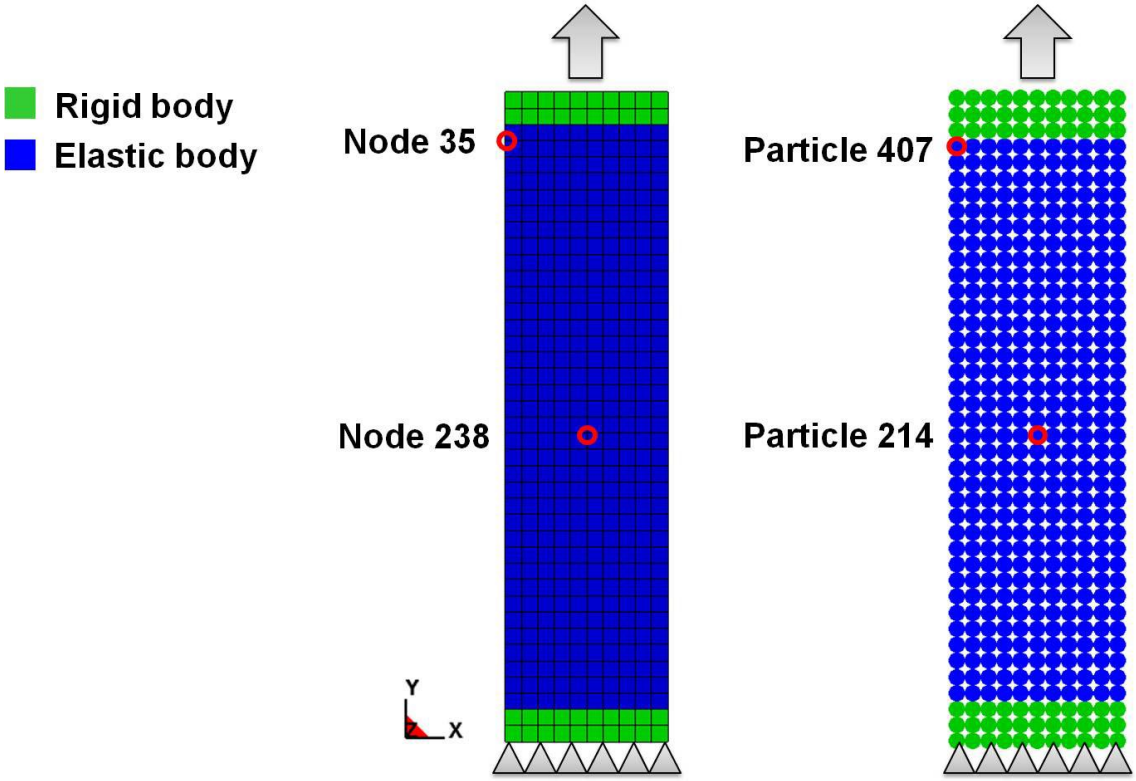
Rigid body
Elastic body
Node 35
Node 238
Particle 407
Particle 214
Y
X

Figure 2(B)

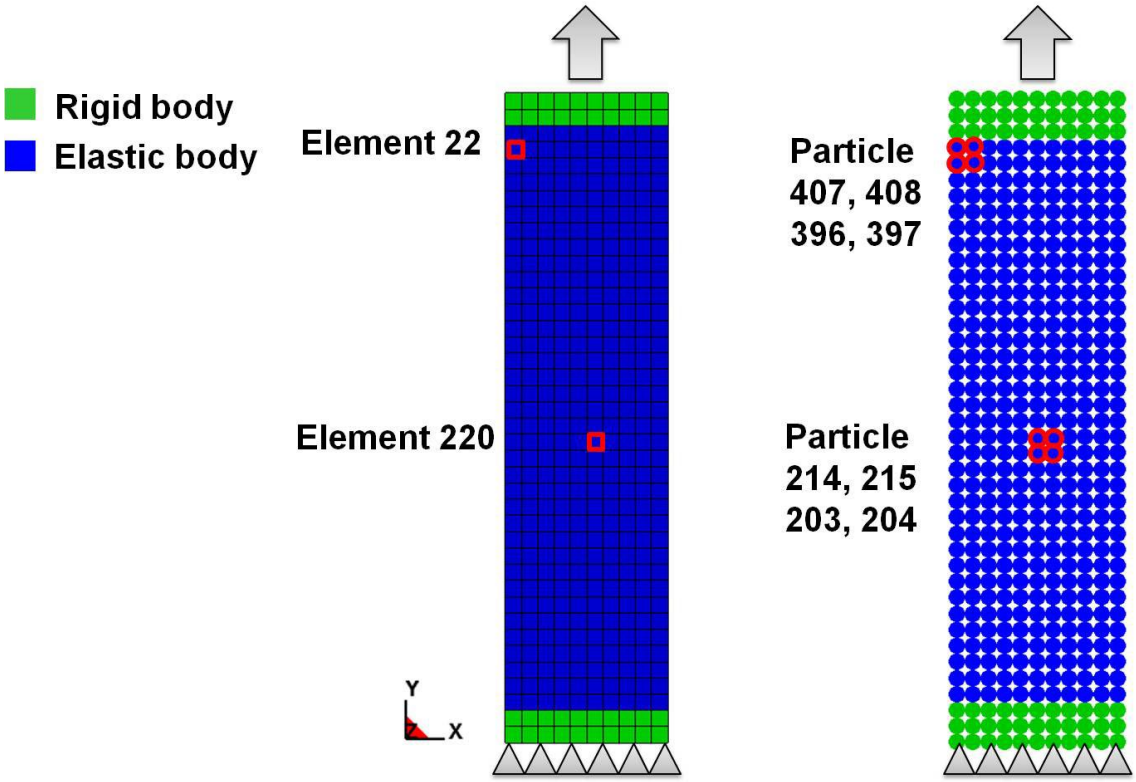
Rigid body
Elastic body
Element 22
Element 220
Y
X
Particle
407, 408
396, 397
Particle
214, 215
203, 204

Figure 3(A)

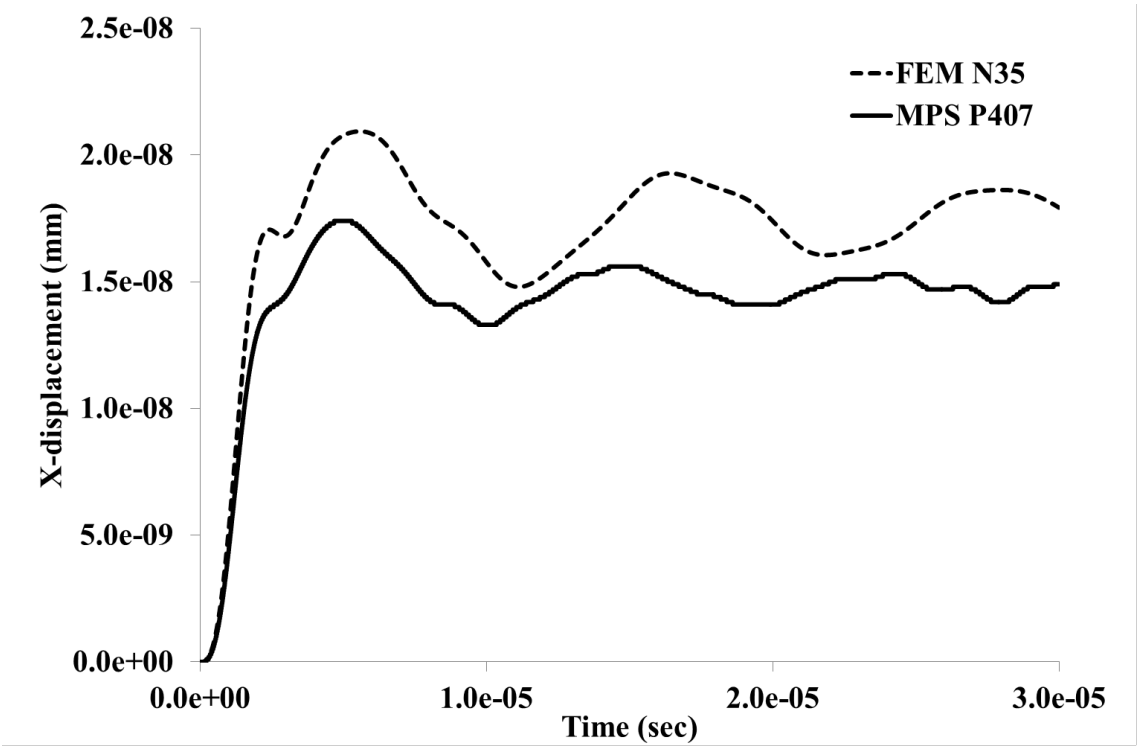
2.5e-08
2.0e-08
1.5e-08
1.0e-08
5.0e-09
0.0e+00
X-displacement (mm)
0.0e+00
1.0e-05
2.0e-05
3.0e-05
Time (sec)
FEM N35
MPS P407

Figure 3(B)

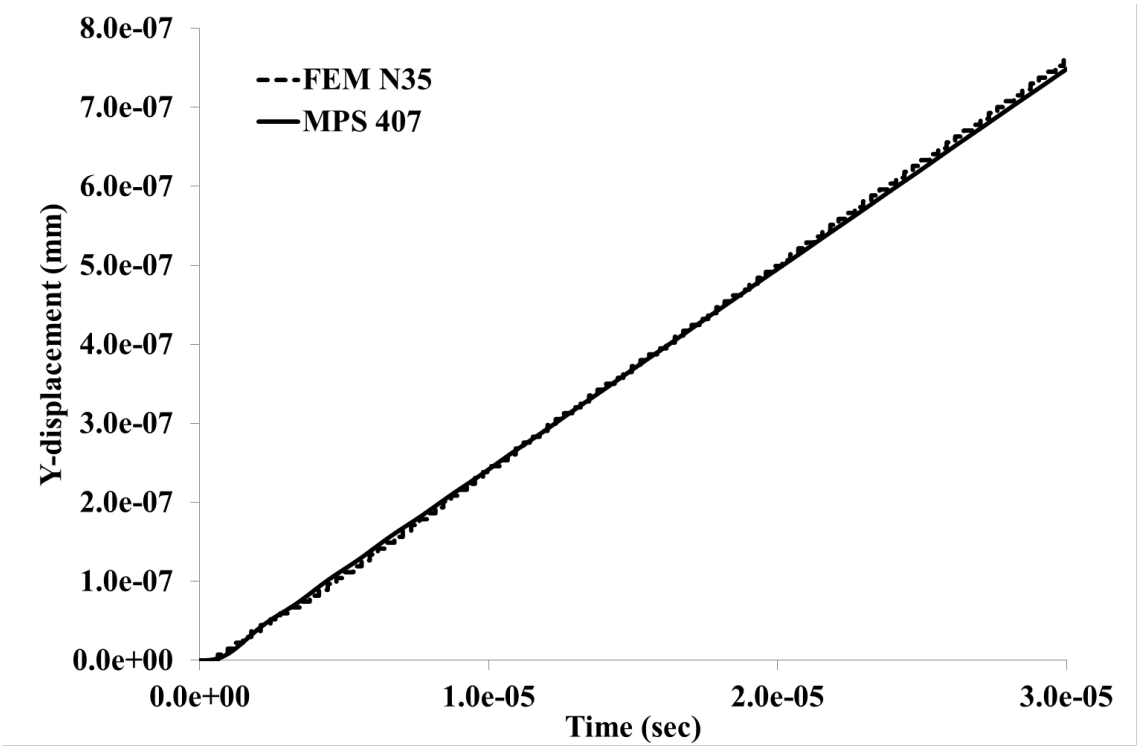
8.0e-07
7.0e-07
6.0e-07
5.0e-07
4.0e-07
3.0e-07
2.0e-07
1.0e-07
0.0e+00
Y-displacement (mm)
FEM N35
MPS 407
0.0e+00
1.0e-05
2.0e-05
3.0e-05
Time (sec)

Figure 3(C)

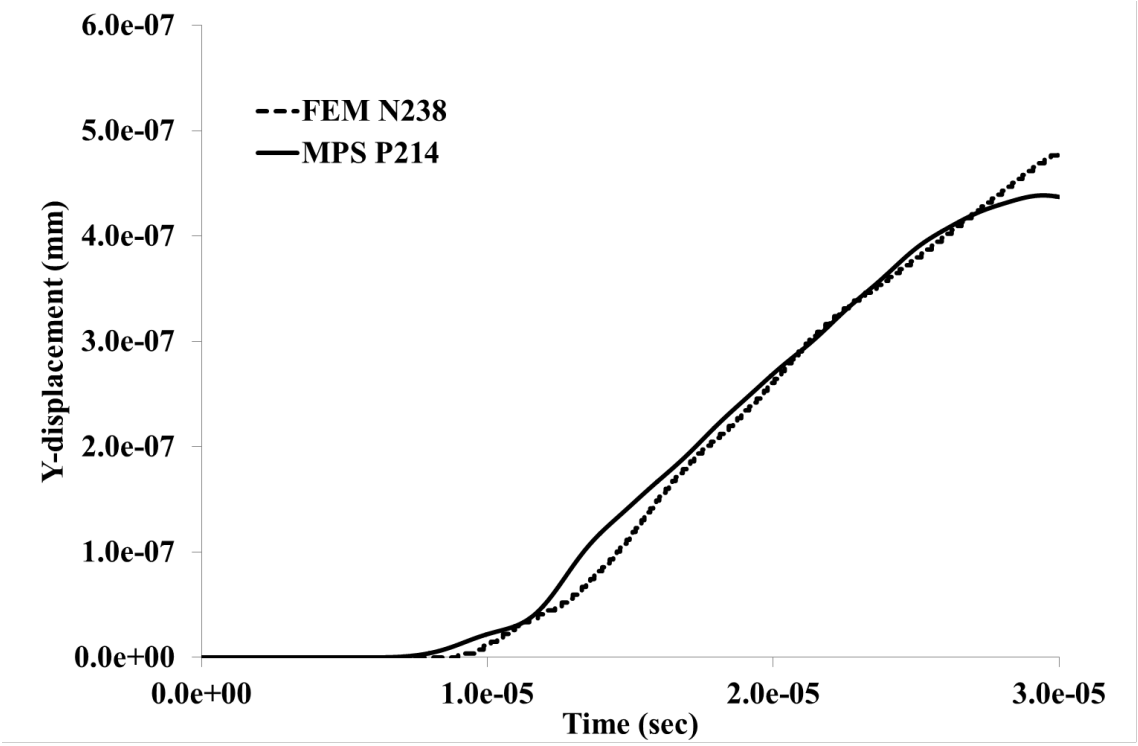
6.0e-07
5.0e-07
4.0e-07
3.0e-07
2.0e-07
1.0e-07
0.0e+00
Y-displacement (mm)
FEM N238
MPS P214
0.0e+00
1.0e-05
2.0e-05
3.0e-05
Time (sec)

Figure 3(D)

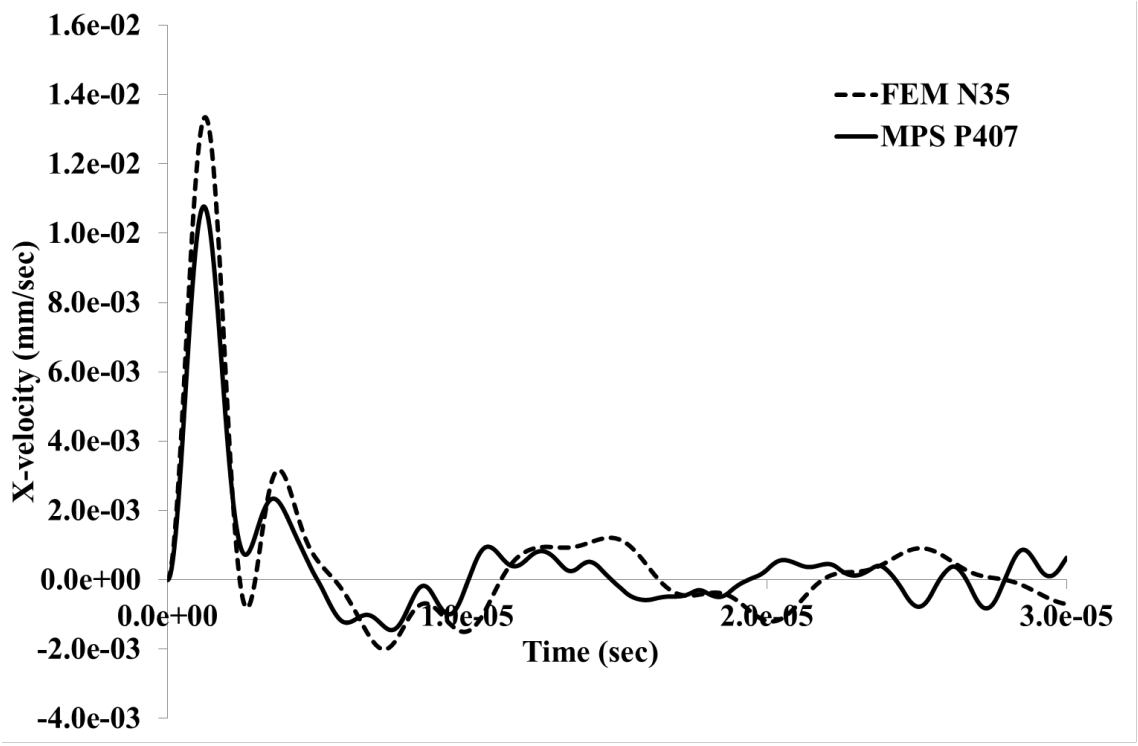
1.6e-02
1.4e-02
1.2e-02
1.0e-02
8.0e-03
6.0e-03
4.0e-03
2.0e-03
0.0e+00
-2.0e-03
-4.0e-03
X-velocity (mm/sec)
0.0e+00
1.0e-05
2.0e-05
3.0e-05
Time (sec)
FEM N35
MPS P407

Figure 3(E)

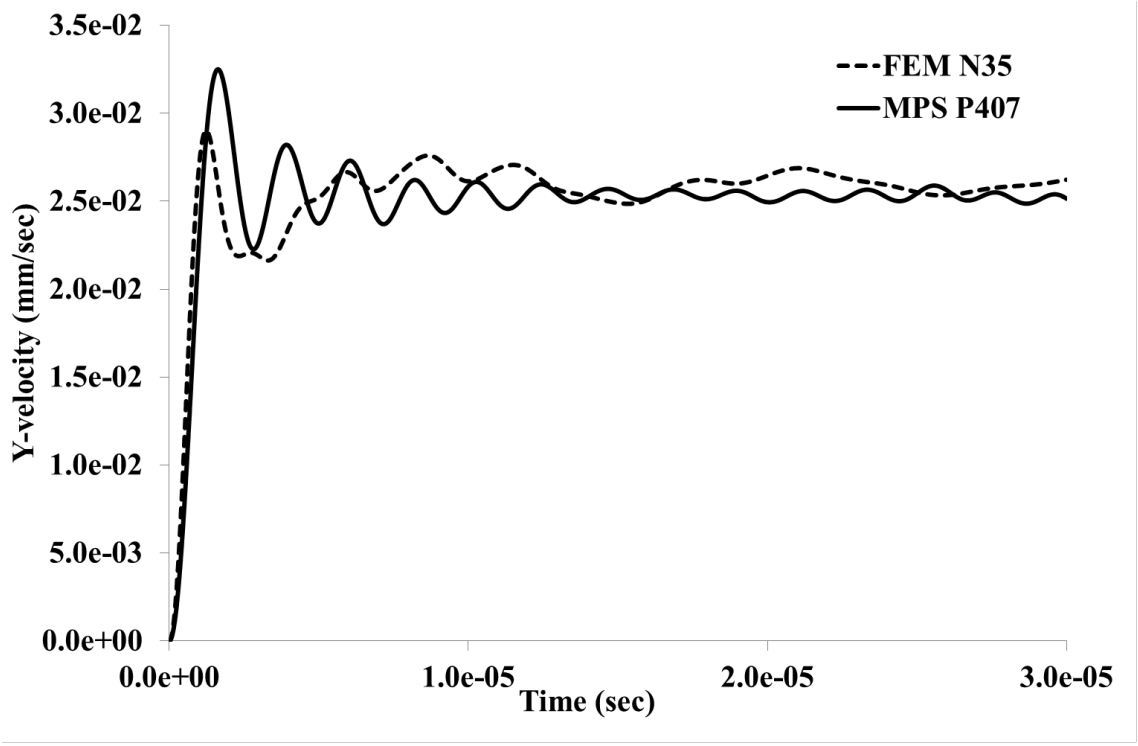
3.5e-02
3.0e-02
2.5e-02
2.0e-02
1.5e-02
1.0e-02
5.0e-03
0.0e+00
Y-velocity (mm/sec)
0.0e+00
1.0e-05
2.0e-05
3.0e-05
Time (sec)
FEM N35
MPS P407

Figure 3(F)

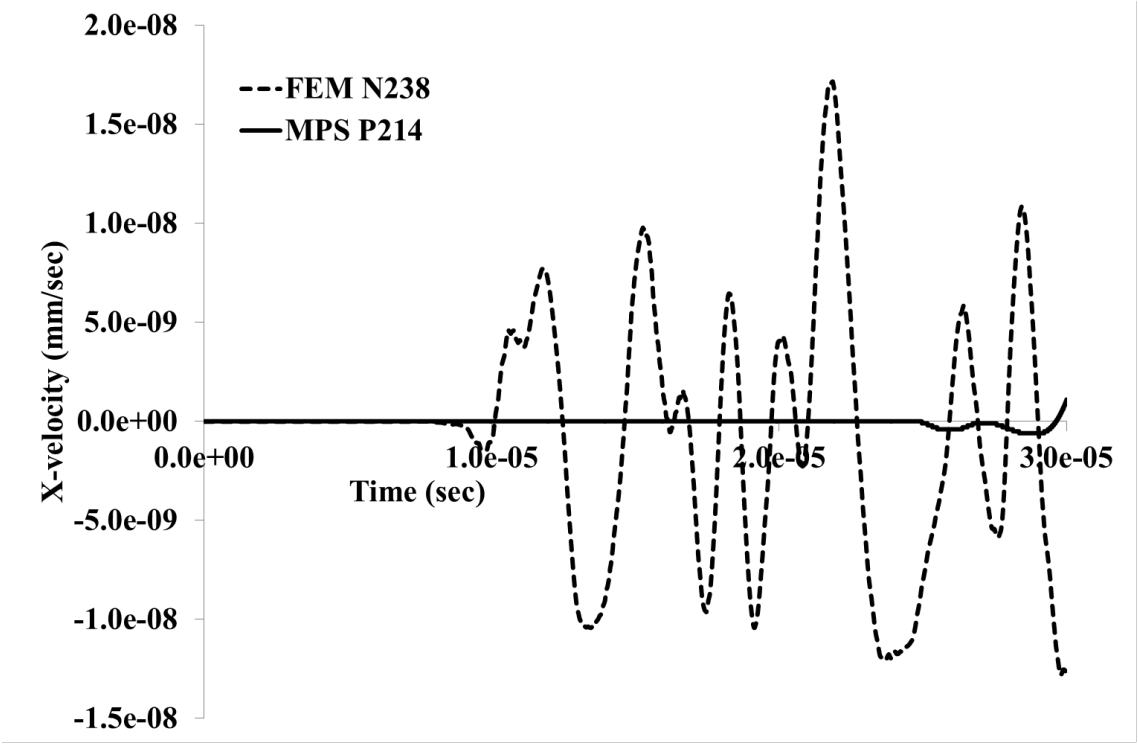
2.0e-08
1.5e-08
1.0e-08
5.0e-09
0.0e+00
-5.0e-09
-1.0e-08
-1.5e-08
X-velocity (mm/sec)
FEM N238
MPS P214
0.0e+00
1.0e-05
2.0e-05
3.0e-05
Time (sec)

Figure 3(G)

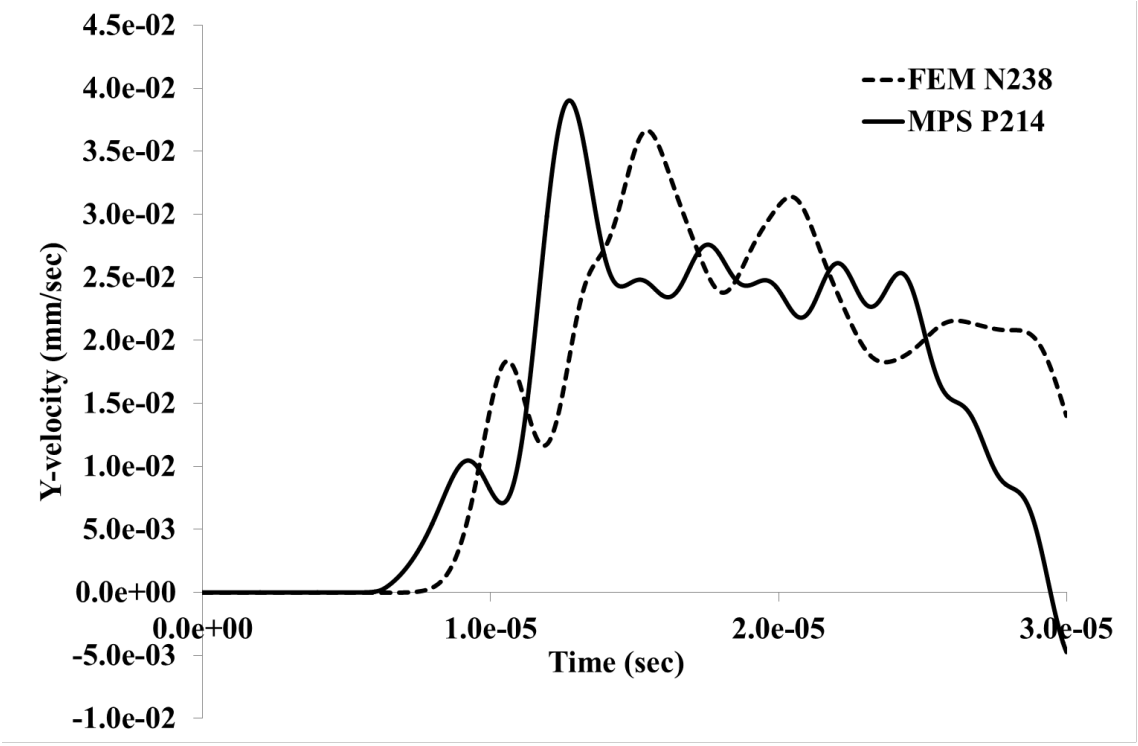
4.5e-02
4.0e-02
3.5e-02
3.0e-02
2.5e-02
2.0e-02
1.5e-02
1.0e-02
5.0e-03
0.0e+00
-5.0e-03
-1.0e-02
Y-velocity (mm/sec)
0.0e+00
1.0e-05
2.0e-05
3.0e-05
Time (sec)
FEM N238
MPS P214

Figure 4(A)

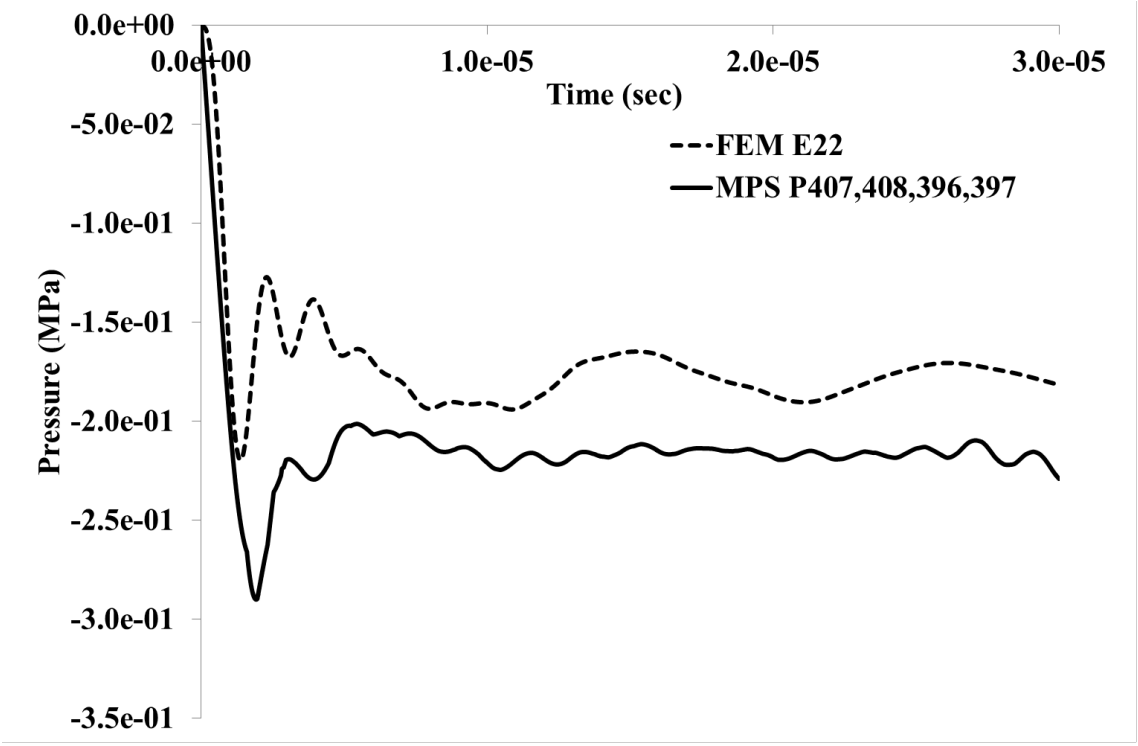
0.0e+00
0.0e+00
1.0e-05
2.0e-05
3.0e-05
Time (sec)
-5.0e-02
-1.0e-01
-1.5e-01
-2.0e-01
-2.5e-01
-3.0e-01
-3.5e-01
Pressure (MPa)
FEM E22
MPS P407,408,396,397

Figure 4(B)

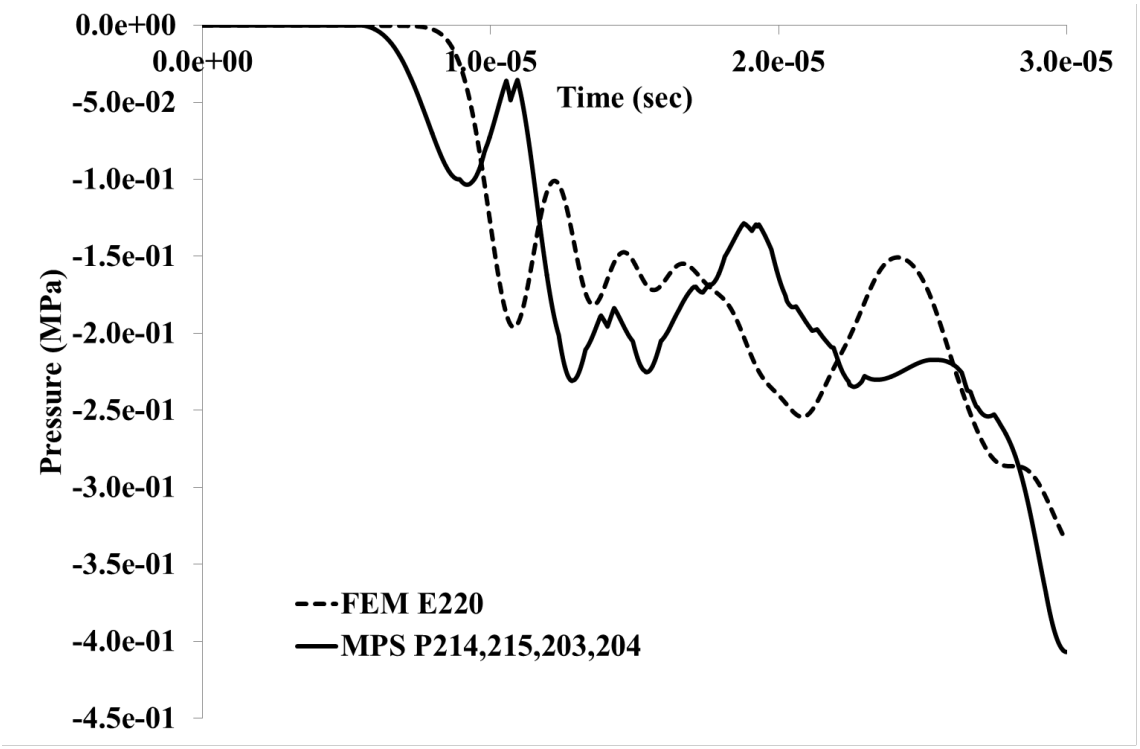
0.0e+00
0.0e+00
1.0e-05
2.0e-05
3.0e-05
Time (sec)
-5.0e-02
-1.0e-01
-1.5e-01
-2.0e-01
-2.5e-01
-3.0e-01
-3.5e-01
-4.0e-01
-4.5e-01
Pressure (MPa)
FEM E220
MPS P214,215,203,204

Figure 4(C)

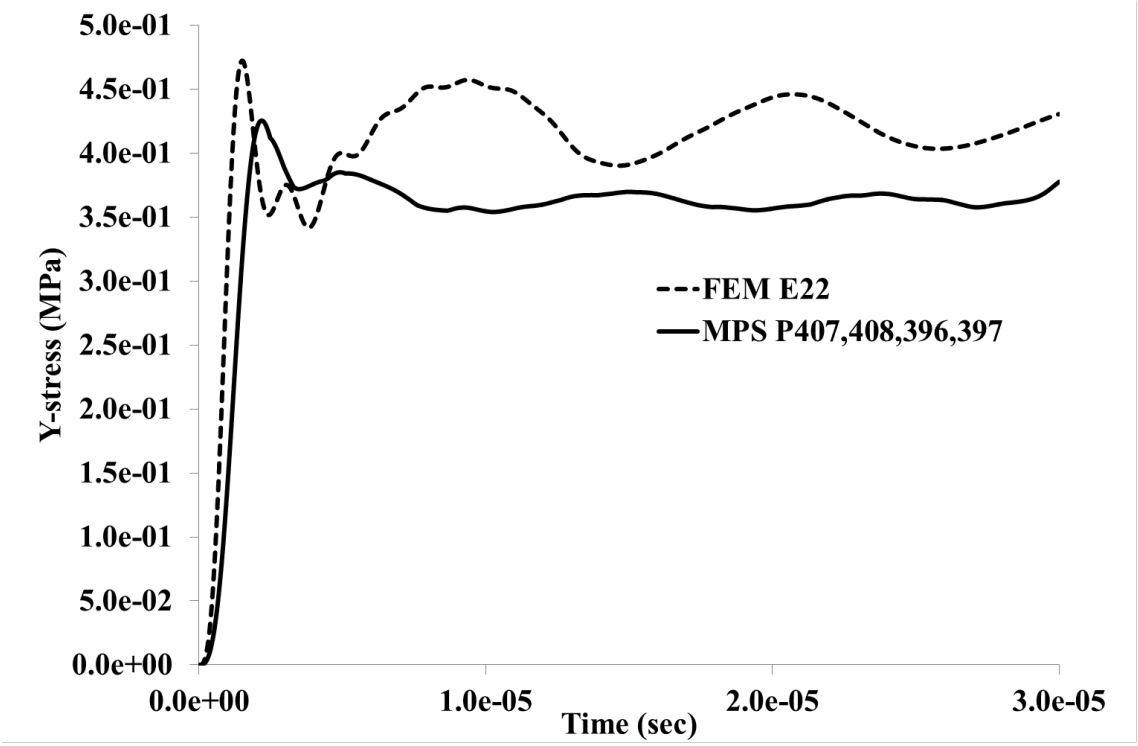
5.0e-01
4.5e-01
4.0e-01
3.5e-01
3.0e-01
2.5e-01
2.0e-01
1.5e-01
1.0e-01
5.0e-02
0.0e+00
Y-stress (MPa)
0.0e+00
1.0e-05
2.0e-05
3.0e-05
Time (sec)
FEM E22
MPS P407,408,396,397

Figure 4(D)

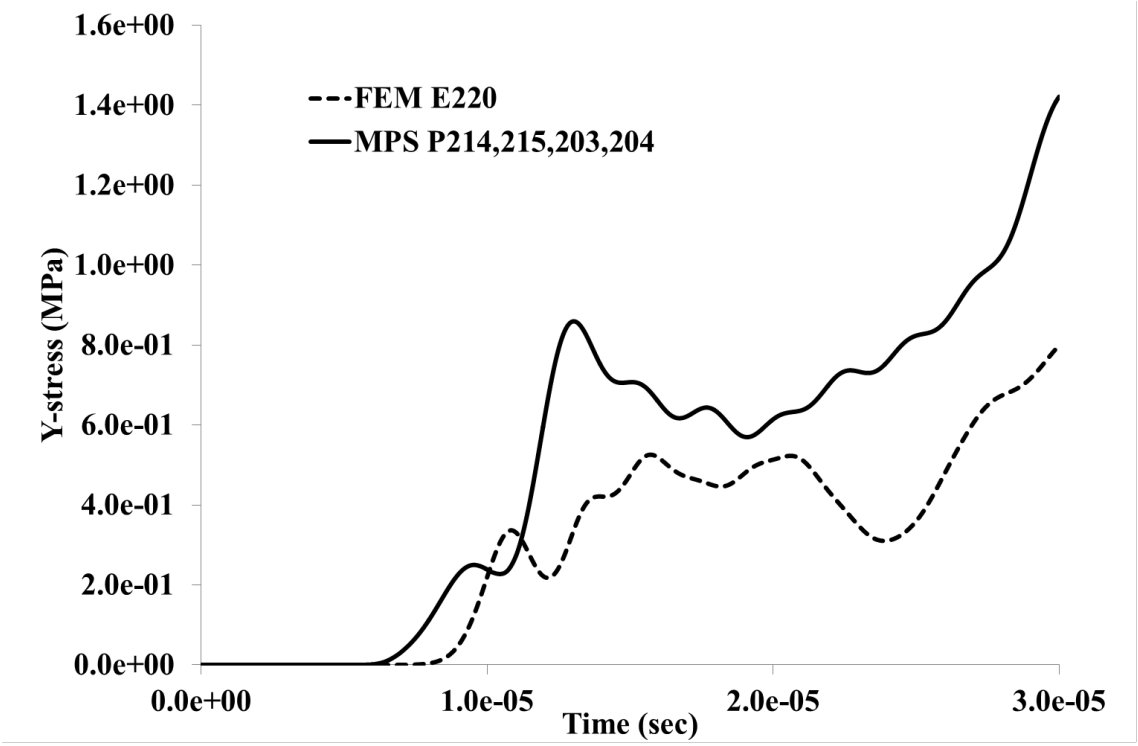
1.6e+00
1.4e+00
1.2e+00
1.0e+00
8.0e-01
6.0e-01
4.0e-01
2.0e-01
0.0e+00
Y-stress (MPa)
FEM E220
MPS P214,215,203,204
0.0e+00
1.0e-05
2.0e-05
3.0e-05
Time (sec)

Figure 5(A)

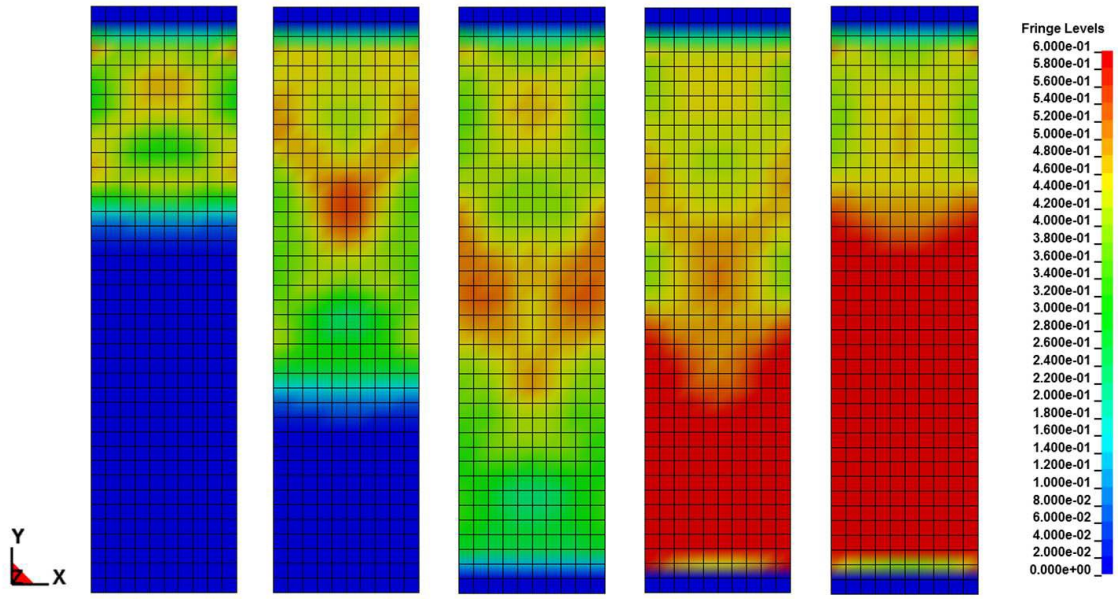
Fringe Levels
6.000e-01
5.800e-01
5.600e-01
5.400e-01
5.200e-01
5.000e-01
4.800e-01
4.600e-01
4.400e-01
4.200e-01
4.000e-01
3.800e-01
3.600e-01
3.400e-01
3.200e-01
3.000e-01
2.800e-01
2.600e-01
2.400e-01
2.200e-01
2.000e-01
1.800e-01
1.600e-01
1.400e-01
1.200e-01
1.000e-01
8.000e-02
6.000e-02
4.000e-02
2.000e-02
0.000e+00
Y
X

Figure 5(B)

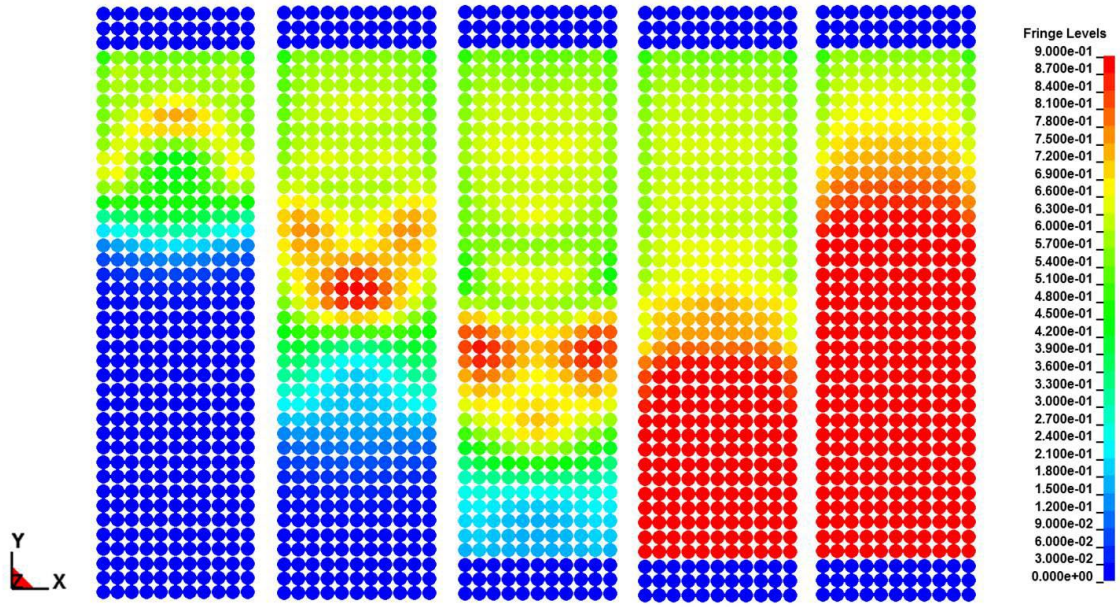
Fringe Levels
9.000e-01
8.700e-01
8.400e-01
8.100e-01
7.800e-01
7.500e-01
7.200e-01
6.900e-01
6.600e-01
6.300e-01
6.000e-01
5.700e-01
5.400e-01
5.100e-01
4.800e-01
4.500e-01
4.200e-01
3.900e-01
3.600e-01
3.300e-01
3.000e-01
2.700e-01
2.400e-01
2.100e-01
1.800e-01
1.500e-01
1.200e-01
9.000e-02
6.000e-02
3.000e-02
0.000e+00
Y
X

Table 1

| | Displacement (mm) | | Velocity (mm/s) | | Pressure (MPa) | Y-stress (MPa) |
|---|---|---|---|---|---|---|
| | x | y | x | y | | |
| N35 and P407 | 4.513e-09 | 1.386e-08 | 2.836e-03 | 7.928e-03 | - | - |
| E22 and P396-397-407-408 | - | - | - | - | 0.143 | 0.203 |
| N238 and P214 | - | 4.346e-08 | 1.718e-08 | 2.254e-02 | - | - |
| E220 and P203-204-214-215 | - | - | - | - | 0.158 | 0.622 |

Table 2

| | Displacement | | Velocity | | Pressure | Y-stress |
|---|---|---|---|---|---|---|
| | x | y | x | y | | |
| N35 and P407 | 0.535** | 1.000** | 0.495** | 0.810** | - | - |
| E22 and P396-397-407-408 | - | - | - | - | 0.155** | -0.544** |
| N238 and P214 | - | 0.991** | -0.630** | 0.757** | - | - |
| E220 and P203-204-214-215 | - | - | - | - | 0.792** | 0.806** |

**SUMMARY**

The study of biomechanics of deformation and fracture of hard biological tissues remains a challenge as variations in mechanical properties and fracture mode may have time dependency. Finite element analysis (FEA) has been widely used but its shortcomings such as its long computation time owing to re-meshing in the simulation of fracture mechanics have warranted the development of alternative computational methods with higher throughput.

The aim of this study was to compare dynamic two-dimensional FEA and moving particle simulation (MPS) when assuming a plane strain condition in modeling human enamel on a reduced scale.

To evaluate the difference between FEA and MPS, the displacement, velocity, pressure, and Y-stress (stress along the Y axis, Fig. 2) output were observed from step 0 to 3000 in intervals of 600 steps.

Simulations were performed under the assumptions of dental enamel being a linear elastic isotropic material and that there is no attenuation of the elastic wave. The results obtained in FEA and MPS had overall agreement, indicating that MPS is suitable for dynamic, structural, and mechanical simulation.

Within the limitation of two-dimensional analysis, we successfully applied MPS to

human enamel tissue on a micro scale and compared displacement, velocity, pressure, and Y-stress results with the results of FEA. The implemented MPS provided acceptable results relative to those of FEA and may be extended to other hard biological tissues.

## FIGURE LEGENDS

**Figure 1** Schematic illustration of plain strain conditions for human enamel at a micro scale.

**Figure 2**

**(A)** Developed model, boundary conditions, and observation points (red circles) for displacement and velocity.

**(B)** Developed model, boundary conditions, and observation areas (red circles) for pressure and Y-stress.

**Figure 3**

**(A)** X-displacement at node 35 and particle 207.

**(B)** Y-displacement at node 35 and particle 207.

**(C)** Y-displacement at node 238 and particle 214.

**(D)** X-velocity at node 35 and particle 207.

**(E)** Y-velocity at node 35 and particle 207.

**(F)** X-velocity at node 238 and particle 214.

**(G)** Y-velocity at node 238 and particle 214.

**Figure 4**

**(A)** Pressure at element 22 and average pressure at particle 407, 408, 396, and 397.

**(B)** Pressure at element 220 and average pressure at particle 214, 215, 203, and 204.

**(C)** Y-stress at element 21 and average Y-stress at particle 407, 408, 396, and 397.

**(D)** Y-stress at element 238 and average Y-stress at particle 214, 215, 203, and 204.

**Figure 5**

**(A)** Y-stress distribution in FEA from step 0 to 3000 in intervals of 600 steps.

**(B)** Y-stress distribution in MPS from step 0 to 3000 in intervals of 600 steps.

**Table 1**

Maximum differences between MPS and FEA

**Table 2**

Spearman's correlation coefficient R between MPS and FEA. (**) denotes statistically

1 significant correlation ($p$<0.001) between MPS and FEA.

**Highlights:**

1. We compared dynamic two-dimensional FEA and moving particle simulation (MPS).
2. We assumed a plane strain condition in modeling human enamel on a reduced scale.
3. We developed two-dimensional models with the same geometry was developed for both MPS and FEA.
4. We tested the models tested in tension generated with a single step of displacement.
5. The MPS and FEA were significantly correlated for all data sets.

.001) between MPS and FEA.